Hindawi
Geofluids
Volume 2021, Article ID 6236455, 10 pages
https://doi.org/10.1155/2021/6236455

Research Article

Hydrogeology Response to the Coordinated Mining of Coal and Uranium: A Transparent Physical Experiment

Tong Zhang,[1,2,3,4] **Xiang He**,[2,3] **Kai Zhang**,[1] **Xiaohan Wang**,[2,3] **and Yang Liu**[2,3]

[1]*State Key Laboratory of Water Resource Protection and Utilization in Coal Mining, Beijing 100000, China*
[2]*State Key Laboratory of Mining Response and Disaster Prevention and Control in Deep Coal Mines, Anhui University of Science and Technology, Huainan, Anhui 232001, China*
[3]*School of Mining and Safety Engineering, Anhui University of Science & Technology, Anhui 232001, China*
[4]*Beijing Key Laboratory for Precise Mining of Intergrown Energy and Resources, University of Mining and Technology (Beijing), Beijing 100083, China*

Correspondence should be addressed to Tong Zhang; 1099731996@qq.com

Received 3 July 2021; Accepted 28 September 2021; Published 8 November 2021

Academic Editor: Hailiang Jia

The migration of fracture and leaching solute caused by mining activity is critical to the hydrogeology. To characterize liquid and solid migration in a mining area of intergrown resources, the coordinated mining of coal and uranium was considered, and a physical experiment based on transparent soil was conducted. A well experimental performance of transparent soil composed of paraffin oil, n-tridecane, and silica gel and the leaching solution comprised of saturated oil red O dye was observed for hydrogeology characterization. An "arch-shaped" fracture zone with a maximum height of 90 m above the mined goaf and a "horizontal-shaped" fracture zone with a fractured depth of 9.97–16.09 m in the uranium-bearing layer were observed. The vertical leachate infiltration of 4.83 m was observed in the scenario of uranium mining prior to coal, which is smaller than those in the scenarios of comining of coal and uranium (10.26 m) and coal mining prior to uranium (16.09 m). A slight strata movement below the uranium was observed, and the leaching solution infiltration in the coal mining area was not observed in a short period in the scenario of uranium mining prior to coal; both of those was presented in the scenarios of comining of coal and uranium and coal mining prior to uranium.

1. Introduction

The natural resource mining of coal, oil, uranium, etc. concerns a series of safety and environmental problems. Visualizing the strata movement, failure mechanism, and seepage distribution attracts numerous attention, and many achievements have been obtained [1–5]. To investigate the mechanism and characteristics of the geotechnical problems, transparent soil, including a refractive index-matched skeleton and a saturating fluid, has been accepted in the field of physical modeling [6, 7]. The internal deformation and flow path in the case of multiscale geotechnical experiments can be appropriately described in a continuous and nonintrusive manner [8–10]. Further, the time-dependent spatial behaviors and seepage features inside the transparent soil can be appropriately measured using optical technologies and image processing techniques, including particle image velocimetry (PIV) and digital image correlation (DIC) [11–13].

The soil skeleton materials and their corresponding fluids, including amorphous silica powder, silica gel, hydrogels, and fused quartz, have been extensively developed to mimic different natural soils [14]. Xu [15] developed the transparent soil, comprising silica gel powder, mineral oil, and n-tridecane, to study the deformation damage mechanism and fracture evolution of the surrounding rock. Ahmed and Iskander [16] evaluated the tunnel construction stability based on the prepared transparent soil and mineral oil solution. Wei et al. [17] introduced transparent cemented soil as a surrogate for the physical modeling of geotechnical problems. Zhang [18] developed a transparent rock similar material, which was applied in the stress and deformation experiments of the tunnel. Ye [19] conducted a 3D crack

growth test using similar materials containing transparent brittle rock, which were similar to the epoxy resin, curing agent, and rosin materials via the high- and low-temperature treatment processes. Fu et al. [20] studied the fracture process based on a new material having a three-dimensional internal fracture surface, which contained a C-type epoxy resin, curing agent, and thin mica sheet. Li et al. [21] developed a type of transparent rock, which was a similar test material and contained a mixed solution of silicon powder and mineral oil (liquid paraffin and n-tridecane).

The intergrown resource mining concerns the stress-fracture-seepage-solute transportation coupling process, which is directly related to groundwater and mining safety. The transparent soil and developed coordinated mining equipment were employed to investigate the development of the mining-induced fracture and leaching solution in this study. Taking coordinated mining of coal and uranium as an example, a physical experiment was conducted in different mining scenarios, and the migration and distribution of the fracture zone and leaching solute were analyzed.

2. Hydrogeology

The intergrown resource deposit of coal and uranium is located in Yijinhuoloqi in the northeast of the Ordos Basin. In the coal mine with a production capacity of 26 million t/a and a mining area of 399.94 km^2, the mining coal seam 3-1 is buried at a depth of 600 m with an average thickness of 3.36 m. The sandstone-type uranium is grown in the Jurassic and located in the east wing of the coal mine with an area of 4.17 km^2. The thickness of the uranium varies from 1.10 m to 7.90 m, and the average thickness of the uranium is 3.44 m. Additionally, the uranium is located above the 3-1 coal seam at a distance of 90–150 m, and the uranium-bearing stratum is a direct aquifer of the 3-1 coal seam. The occurrence of coal and uranium is shown in Figure 1, and the specific hydrogeology is shown in Figure 2.

3. Mathematical Model of the Physical Experiment

To characterize the hydrogeology of the intergrown resource, a mathematical model as a function of a hydromechanical coupling equation, elasticity equilibrium equation, and effective stress equation is employed as

$$\begin{cases} K_x \dfrac{\partial^2 p}{\partial x^2} + K_y \dfrac{\partial^2 p}{\partial y^2} + K_z \dfrac{\partial^2 p}{\partial z^2} = S\dfrac{\partial p}{\partial t} + \dfrac{\partial e}{\partial t} + W, \\ \sigma_{ij,i} + X_j = \rho \dfrac{\partial^2 u_i}{\partial t^2}, \\ \sigma_{ij} = \overline{\sigma_{ij}} + \alpha\delta p, \end{cases} \tag{1}$$

where K_x, K_y, and K_z are the permeability coefficients in the Cartesian system, and $K_x = K_y = K_z$ is assumed; P is the hydraulic pressure; S is the water storage coefficient; W is the source-sink term; e is the volume strain; σ_{ij} is the total stress tensor; $\overline{\sigma_{ij}}$ is the effective stress tensor; X_j is the volume force; ρ is the density; α is Biot's effective stress coefficient; and δ is the Kronecker symbol.

Combining the elasticity balance equation, geometric equation, and physical equation, the stress and strain components are eliminated, and the displacement equation is obtained by

$$\begin{cases} G\nabla^2 u + (\lambda + G)\dfrac{\partial e}{\partial x} + X = \rho \dfrac{\partial^2 u}{\partial t^2}, \\ G\nabla^2 v + (\lambda + G)\dfrac{\partial e}{\partial y} + Y = \rho \dfrac{\partial^2 v}{\partial t^2}, \\ G\nabla^2 w + (\lambda + G)\dfrac{\partial e}{\partial z} + Z = \rho \dfrac{\partial^2 w}{\partial t^2}, \end{cases} \tag{2}$$

where $\nabla^2 = (\partial^2/\partial x^2) + (\partial^2/\partial y^2) + (\partial^2/\partial z^2)$ is the Laplace operator notation; $G = E/2(1+\mu)$ is the shearing modulus of elasticity; $\lambda = \mu E/(1+\mu)(1-2\mu)$ is Lamet's constant; $e = (\partial u/\partial x) + (\partial v/\partial y) + (\partial w/\partial z)$ is the volumetric strain; and X, Y, Z are the volume force in the Cartesian coordinate system.

The coefficients in the prototype characterized by $(')$ and physical model represented by $('')$ are suitable in the given mathematical model: $C_G = G'/G''$, $C_E = E'/E''$, $C_l = x'/x''$, $C_\lambda = \lambda'/\lambda''$, $C_e = e'/e''$, $C_u = u'/u''$, $C_\gamma = X'/X''$, $C_\rho = \rho'/\rho''$, $C_t = t'/t''$, $K' = C_K K''$, $S' = C_S S''$, $Q' = C_Q Q''$, $y' = C_l y''$, $z' = C_l z''$, $\partial e'/\partial x' = (1/C_l)(\partial e''/\partial x'')$, $\nabla^2 u' = (C_u/C_l^2)\nabla^2 u''$, and $\partial^2 u'/\partial t'^2 = (C_u/C_t^2)(\partial^2 u''/\partial t''^2)$, where C_i is the similarity coefficient. Based on a similar principle [22], the following expressions are given:

$$C_G \frac{C_u}{C_l^2} = C_\lambda \frac{C_e}{C_l} = C_G \frac{C_e}{C_l} = C_\gamma = C_\rho \frac{C_u}{C_t^2}, \tag{3}$$

$$C_K \frac{C_P}{C_l^2} = C_S \frac{C_p}{C_t} = \frac{C_e}{C_t} = C_w. \tag{4}$$

(1) Geometric similarity: $C_u = C_e C_l$ and $C_e = 1$ were assumed and $C_u = C_l$ was obtained

(2) Stress similarity: combining $C_G C_e = C_\gamma C_l$, $C_e = 1$, and the similarity principle and the homogeneous principle of dimension, the $C_G = C_\lambda = C_E = C_p = C_\gamma C_l$ was obtained

(3) Time similarity: integrating $C_\gamma = C_\rho C_g$, $C_u = C_e C_l$, $C_g = 1$, and $C_e = 1$ into $C_\gamma = C_\rho(C_u/C_t^2)$, then $C_t = \sqrt{C_l}$ was obtained

(4) Loading similarity: integrating $K_x = K_y = K_z = K$ into equation (1), then $C_e = 1$, $C_p = C_\lambda C_l$, and $C_t = \sqrt{C_l}$ were obtained

(5) Source and sink term similarity: $C_w = 1/\sqrt{C_l}$

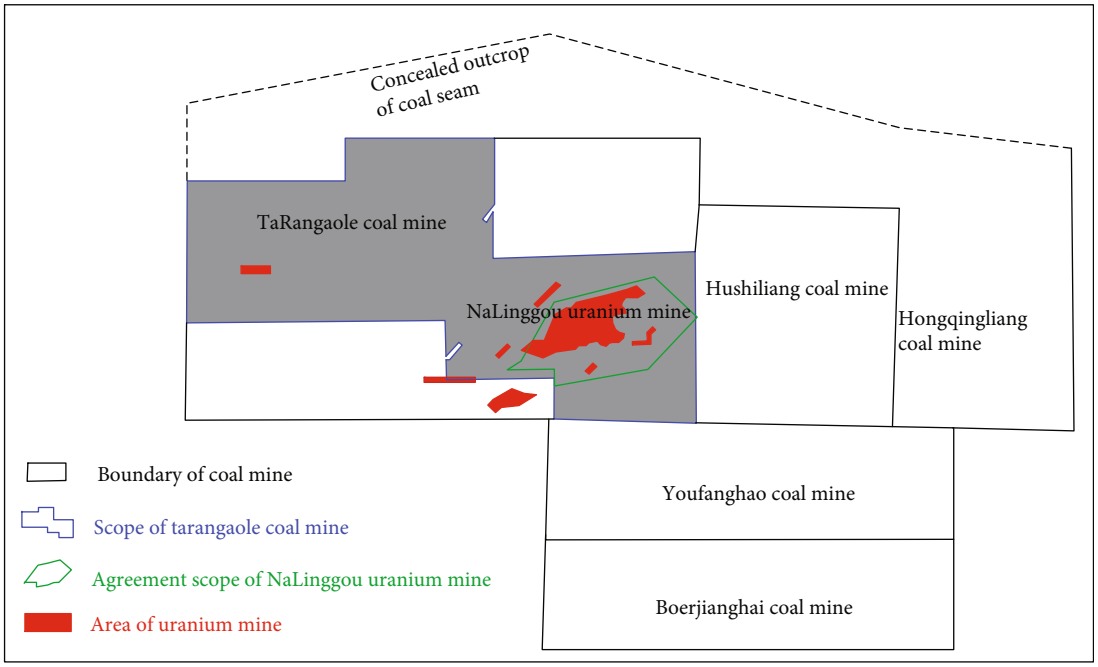

Figure 1: The spatial distribution of coal and uranium in the Ordos Basin.

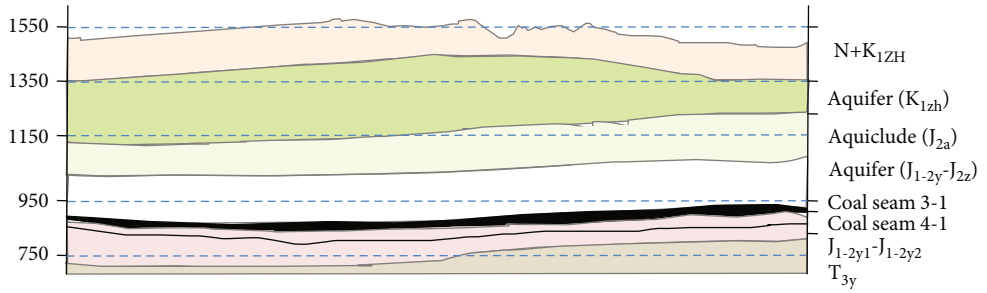

Figure 2: Hydrogeology condition of the coal and uranium reservoir.

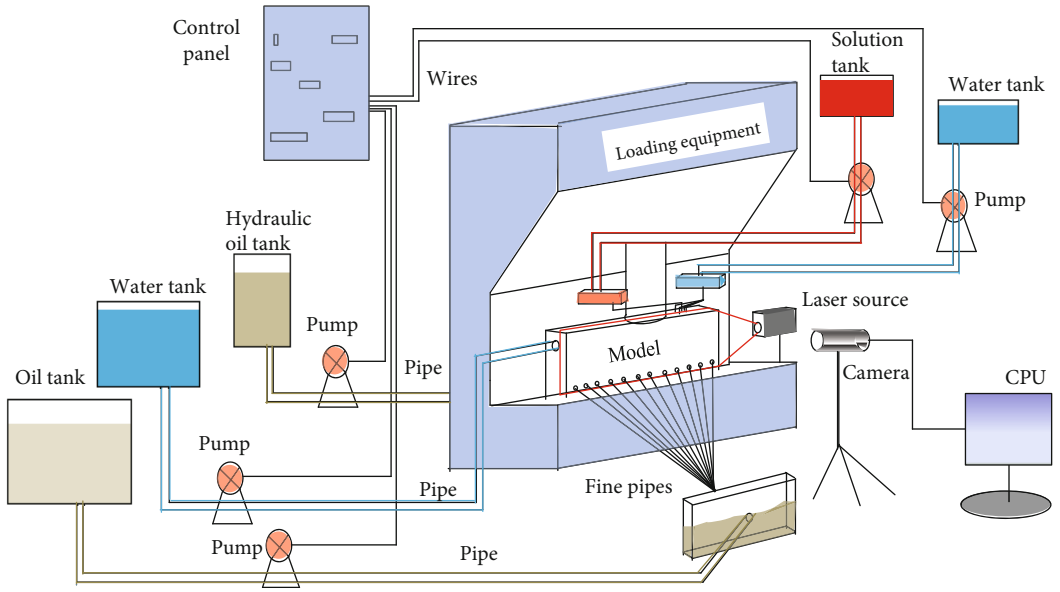

Figure 3: Schematic diagram of coordinated mining equipment.

Table 1: Key technical parameters of the equipment.

Category	Power	Stress/pressure	Measuring range	Accuracy	Flow rate	Operating system
Loading pump	5.5 kW	10 t	400 mm	0.1 mm	—	PLC
Fluid pump	1 kW	0-10 MPa	—	0.01 mL	0-1.2 L/minute	PLC

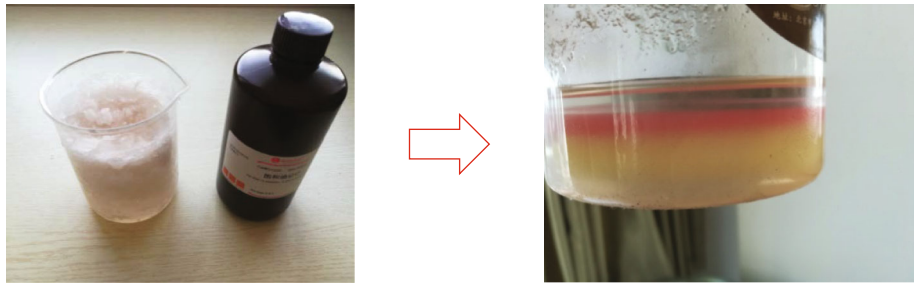

Figure 4: Preparation of the leaching solution.

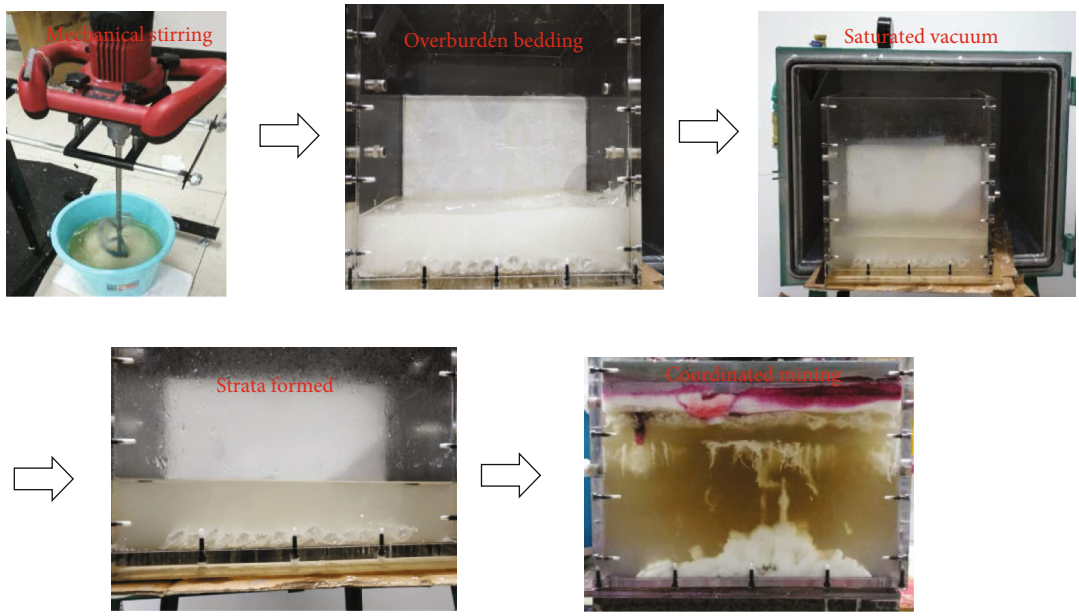

Figure 5: Preparation process of the transparent strata.

(6) Water storage coefficient similarity: $C_S = 1/C_\gamma\sqrt{C_l}$

(7) Permeability similarity: $C_K = \sqrt{C_l}/C_\gamma$

4. Physical Experiment

4.1. Experiment Setup. The geological and hydrology properties were characterized by the transparent soil and leaching solution. The behaviors of fracture development and fluid migration were studied in different mining scenarios. A "seven-point" pattern technology was adopted for the in situ leaching of uranium. The space of pumping wells is set to 30 m, the pumping volume is set to 8 m^3/h, and the coal mining speed is assumed as 16 m/d.

The experiment equipment is composed of the control, loading, and monitoring systems, and a good performance function for the in situ leaching of uranium and coal mining was developed, as shown in Figure 3. In detail, the underground mining of coal and in situ leaching of uranium were performed by hydraulic pumping. The seepage migration, fracture movement, and strata displacement were captured by the monitoring system. And the specific technical parameters are shown in Table 1.

The physical model includes transparent acrylic glass and is sealed by bolts and colloids, and the dimension is 40 cm × 20 cm × 40 cm (length × width × height). The transparent soil is prepared by aggregate particles and saturated liquid. The aggregate particle was made by the mixture of 200–300- and 20–40-mesh silica gel powder, and the

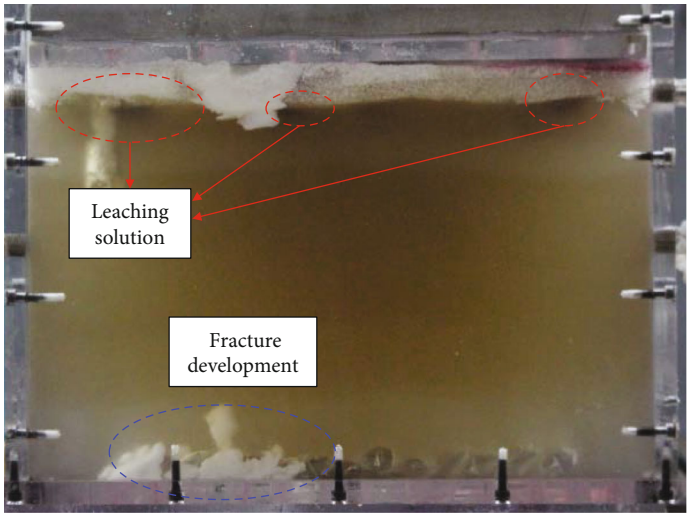

(a) 48 m

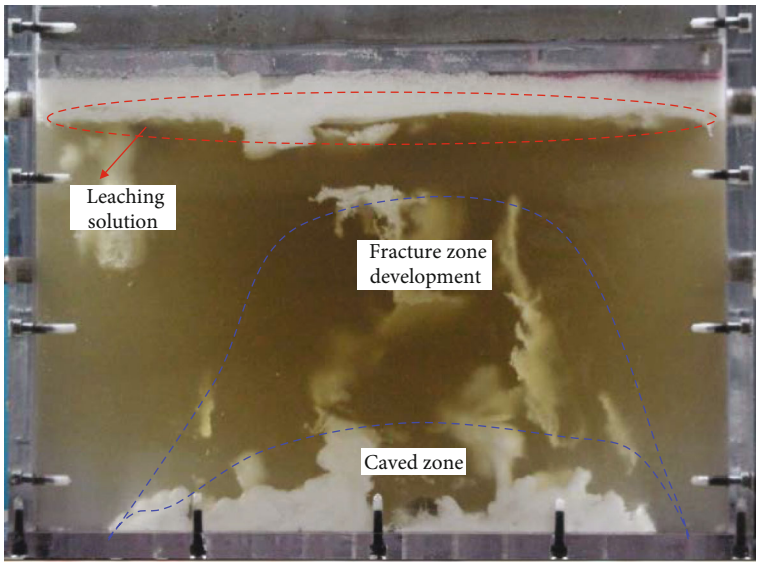

(b) 112 m

Figure 6: Continued.

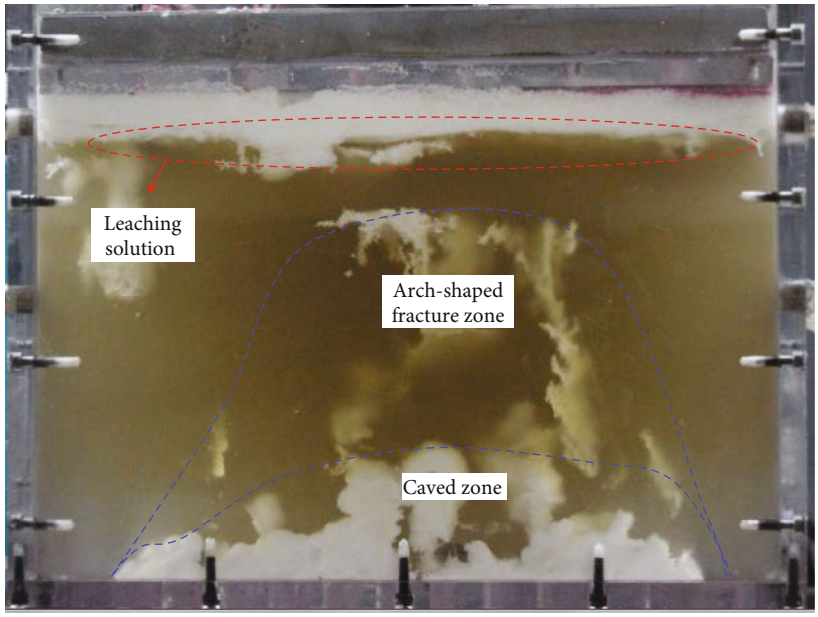

(c) 132 m

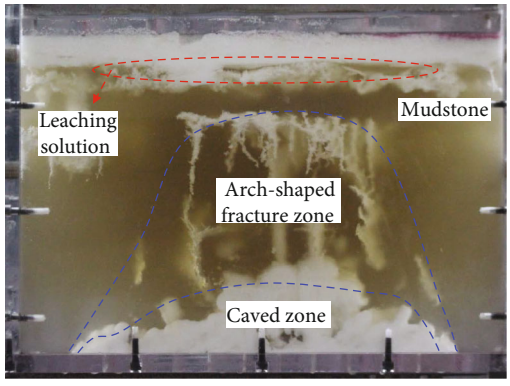

(d) 150 m

Figure 6: Development of fracture field and migration of leaching solution.

saturated liquid was made by the mixture of paraffin oil and n-tridecane.

4.2. Experimental Procedure. The sandy mudstone layer, conglomerate aquifer, and coarse-grained sandstone layer were characterized by transparent soil. The coal seam was described by an oil bag located in the bottom of the physical model. The sandy mudstone layer was characterized by a mixture of 200–300-mesh silica gel powder and mineral oil. The conglomerate aquifer and coarse-grained sandstone were characterized by a mixture of 200–300- and 20–40-mesh silica and mineral oil, respectively. The preparation procedure is shown in Figure 4, and the specific experiment steps are shown:

(1) The saturated liquid was obtained by the mixture of paraffin oil and n-tridecane at a mass ratio of 0.85 : 1. Subsequently, the silica gel powder and saturated liquid were mixed in a mass ratio of 1 : 0.65, and the mixture was stirred using the stirrer for 1 h

(2) The mixture was poured into the transparent abrasive tool to be vacuumized and saturated for 12 h until the bubbles of the material completely disappeared. Subsequently, the mixture was consolidated with respect to a certain amount of mechanical stress for 7 days until the transparent material of the sandy mudstone, conglomerate aquifer, and coarse-grained rock approached the physical strength. Further, the transparent rock layer presented appropriate transparency with a refractive index of 1.42

(3) The saturated oil red O dye and saturated liquid were mixed and retained for 24 h. Then, the solution tracer was obtained as the in situ leaching solution of uranium, as shown in Figure 5

(4) For uranium mining prior to coal, in situ leaching was conducted with the prepared solution tracer using a pumping system. For the scenario of the comining of uranium and coal, the coal seam was mined at a rate of 16 m/d through the pumping fluid

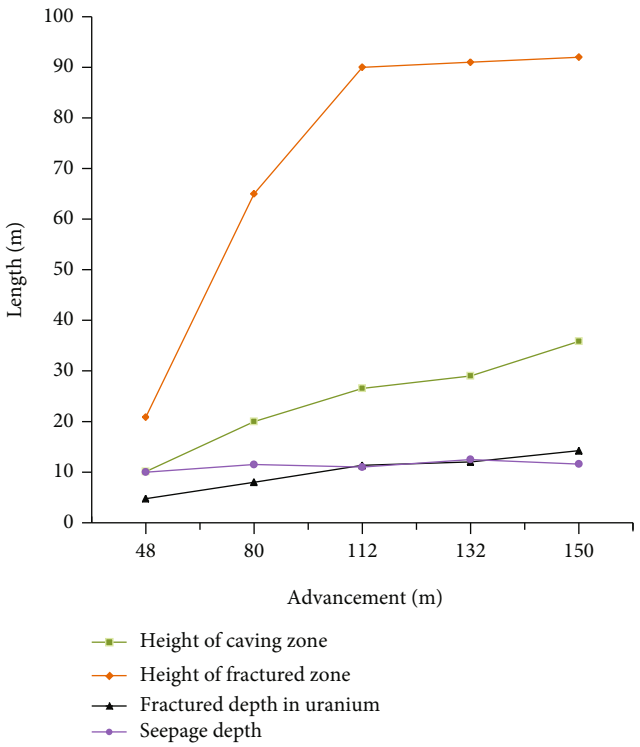

FIGURE 7: Correlation between the coal mining and development of the fracture and seepage zone.

from the oil bag, and the in situ leaching was conducted with the solution tracer using a pumping system. For the scenario of coal mining prior to uranium, the coal seam was initially mined, and the stability of the mining-induced fractured zone was obtained; then, the in situ leaching was performed using the solution tracer

5. Results and Analyses

5.1. Hydrogeology Response to the Comining of Coal and Uranium. During the coordinated mining of coal and uranium, the fracture growth and the solution diffusion were investigated. The specific characteristics of multifield coupling are shown in Figures 6 and 7.

In Figure 6, a "cone-shaped" leaching solution diffusion area around the injection well was observed, as the in situ leaching of uranium at a constant speed of 0.14 m/s. The leaching solution diffused and was transported from the injection well to the pumping well under the effect of the negative pressure. With the advancement of coal mining, the fracture zone and caving zone could be observed in the sandy mudstone above the coal seam. In addition, a "horizontal-shaped" fracture zone was observed in the uranium-bearing layer due to the hydraulic and mechanical fracturing effect. In Figure 7, an increasing trend in the height of the fractured zone and the caving zone and fractured depth was presented, and seepage depth varied around 11 m, as the process of the in situ leaching of uranium. As the coal mining advanced to 48 m, the height of the caving zone approached to 10 m, the height of the fractured zone had grown into 21 m, and the fractured depth evolved into 4.77 m. Meanwhile, the uranium was normally mined, and a 10 m vertical infiltration of leaching solution along the horizontal direction was observed. As the coal mining advanced to 112 m, the height of the caving zone is 26.6 m and the maximum height of the fractured zone is 90 m above the coal goaf. Further, a plastic zone with a length of 20 m was formed in front of the mining face, as shown in Figure 6(b), and a balanced horizontal flow state was obtained with a seepage depth of 11 m and a fracture depth of 11.35 m. As the mining advanced to 150 m, the maximum height of 90 m was maintained with respect to the fractured zone; in contrast, the height of the caving zone is 35.8 m. In addition, a fracture depth of 14.2 m and a seepage depth of 11.6 m are obtained. Further, the stability of the horizontal flow was maintained with respect to the in situ leaching, and the increase in vertical infiltration of the leaching solution was presented. Figure 6(d) shows that the morphology of the fractured zone is characterized by an "arched-shape" structure and the maximum height of the fractured zone is 90 m, as the mining advanced to 150 m. The decrease in fracture zone height from the middle to the end of the stope was presented. No obvious vertical infiltration was observed, as the in situ leaching was performed.

The vertical infiltration of the solution was not obvious in the scenario of the comining of coal and uranium; however, the horizontal and dynamic movements of the solution were observed between the injection well and the pumping well. A fracture zone characterized by the existence of an "arched-shape" structure was observed in the stope, and the stability was maintained for a long time. The maximum height is 90 m, which is 20 times the coal seam thickness. The "arched-shape" boundary of the fracture zone is observed under the no-key-layer condition in the overlying strata, and the coal mining was protected under the "arched-shape" structure.

5.2. Comparison of the Different Mining Scenarios of Coal and Uranium. The diffusion of the leaching solution, the development of a mining-induced fracture zone, and the influence of convection and dispersion of the underground fluid on the diffusion of the leaching solution are presented in Figures 8 and 9.

Figure 8(b) presents that the horizontal movement dominated the distribution of the leaching solution and that vertical infiltrate cannot be formed in the scenario of uranium mining prior to coal. This illustrates that the pressure difference between the coal seam and uranium-bearing strata plays an important role in the distribution of the leaching solution. For the comining of coal and uranium, the fracture zone, characterized by an "arched-shape" morphology, was generated with the advance of coal mining, as shown in Figure 8(c). Further, the stability of the uranium deposit was observed based on the protective effect of the undisturbed layer located below the uranium deposit. The maximum penetration depth of the solution was limited, and the vertical penetration behavior of the solution was not observed in a short period. The accelerated infiltration of

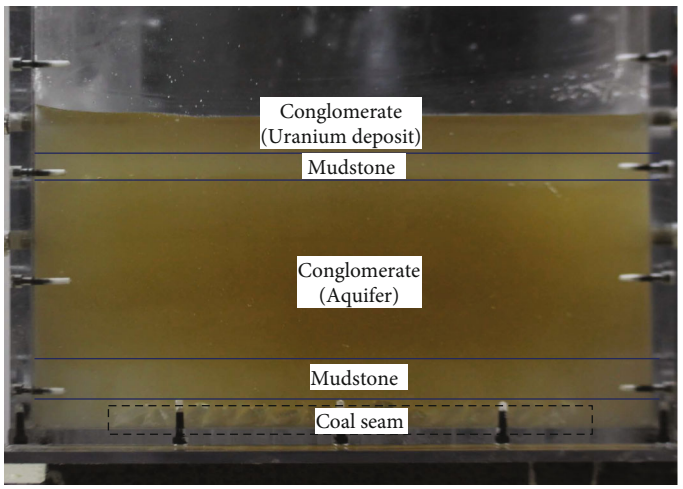

(a) Hydrogeology of the coal and uranium

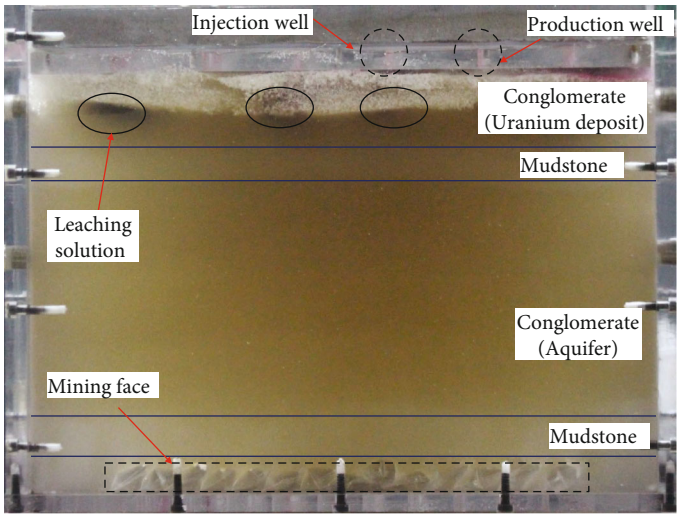

(b) In situ leaching of uranium

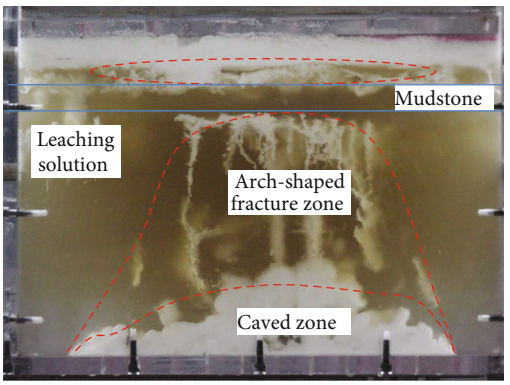

(c) Comining of coal and uranium

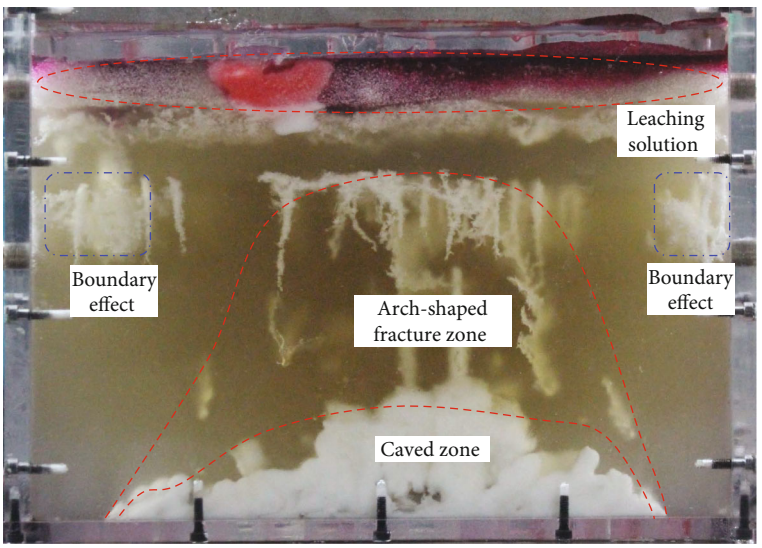

(d) Coordinated mining of coal prior to uranium

Figure 8: Development of the fracture and migration of leaching solution in different mining scenarios.

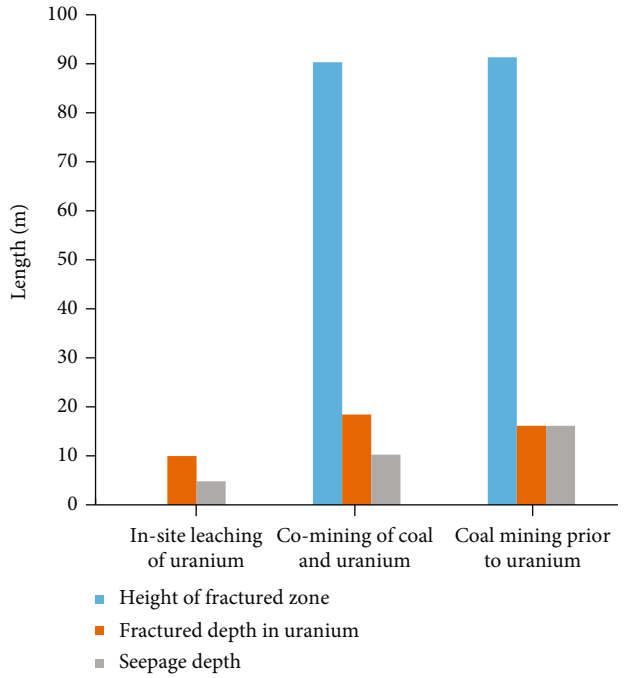

Figure 9: Comparison in the development of fracture and seepage for coordinated mining of coal and uranium.

the solution influenced by the convection effect would be presented in the goaf, as the solution approached the fracture zone in a long period.

Figure 9 shows that a stable 90 m height of the fractured zone was presented in the comining of coal and uranium and coal mining prior to uranium. The fracture depth in the uranium layer in the comining of coal and uranium was larger than that of coal mining prior to uranium and uranium mining prior to coal. However, the seepage depth of the leaching solution in coordinated mining of coal prior to uranium was higher than that in the comining of coal and uranium and uranium mining prior to coal. The maximum fractured depth in the uranium layer was observed in the comining of coal and uranium, because the physical influence and hydraulic fracturing effect caused by coal mining dynamically changed the hydrogeology. Considering the time-dependent effect, the maximum seepage depth was observed in coal mining prior to uranium. The vertical infiltration of the leaching solution was limited to 10–12 m because of the presence of an undisturbed layer during uranium mining in the uranium prior to coal.

6. Discussion

The geotechnical mechanics and permeability of the transparent soil composed of the different skeletons and saturating fluids were studied [7, 14]. And the displacement in embankment road, tunneling, and slope slipping were investigated using the transparent soil [1–5, 23]. However, the development of the mining-induced fracture and leaching solute was rarely characterized by the transparent soil. In this study, the hydrogeology of intergrown resources was described by transparent soil, which comprises paraffin oil, n-tridecane, and silica gel in different mass ratios. The coordinated mining of coal and uranium in different scenarios was performed. The hydrogeology response characterization with respect to the mining can be given as follows:

(1) Considering a matching refractive index, the sandy mudstone was characterized by the mixture of 200–300-mesh silica gel powder and mineral oil; the conglomerate aquifer and coarse-grained sandstone were represented by 200–300- and 20–40-mesh silica gel powder and mineral oil

(2) The mining-induced fracture zone was well characterized by the "white zone" caused by air, and the leaching solution was characterized by the saturated red O dye

(3) The "arch-shaped" fractured zone exhibits a maximum height of 90 m, and the "horizontal-shaped" fractured zone exhibits a maximum height of 14.24 m in the uranium-bearing layer. The leaching solution seepage depth of 12 m was determined by the distribution of the saturated red O dye

(4) The difference in the scope of the fractured zone and seepage area was characterized by the white zone and red zones

7. Conclusions

Based on the physical experiment through transparent soil, the diffusion and migration of the in situ leaching solution and the development of mining-induced fracture zones were observed in different mining scenarios of coal and uranium, and the main conclusions are given:

(1) The hydrogeology was appropriately characterized by a mixture of silica gel powder and mineral oil. The sandy mudstone was characterized by a mixture of 200–300-mesh silica gel powder particles with low permeability. The conglomerate aquifer was characterized by 20–40-mesh silica gel powder. And the mud pebble was characterized by a mixture of 200–300- and 20–40-mesh silica gel powder

(2) With the oil separation and air diffusion along the fracture net, a white zone covering the mining-induced fracture zone was observed; the migration of the leaching solution was characterized by the saturated oil red O dye. A fracture zone characterized by an "arch-shape" morphology was observed with a maximum height of 90 m above the mined goaf, and the mining face was protected by the "arch-shape" structure. "Horizontal-shaped" fracture zones with depths of 9.97, 18.4, and 16.09 m were observed in the uranium-bearing layer for the scenario of uranium prior to coal, comining of coal and uranium, and coal mining prior to uranium, respectively

(3) A smaller leaching solution vertical infiltration of 4.83 m was observed, compared with those of

10.26 m in the comining of coal and uranium and 16.09 m in coal mining prior to uranium. The layer below uranium was stable, and the leaching solution infiltration in the coal mining area was not observed in a short time for coordinated mining in different scenarios

Data Availability

The data used to support the findings of this study are included within the article.

Conflicts of Interest

The authors declared that they have no conflicts of interest to this work.

Acknowledgments

This study was supported by the Open Fund of State Key Laboratory of Water Resource Protection and Utilization in Coal Mining (Grant No. GJNY-18-73.7), National Youth Science Foundation (No. 51904011), Anhui Provincial Natural Science Foundation (No. 1908085QE183), Anhui University Scientific Research Foundation (No. QN2018108), and Institute of Energy, Hefei Comprehensive National Science Center (Grant No. 21KZS216).

References

[1] E. D. Guzman and M. Alfaro, "Modelling a highway embankment on peat foundations using transparent soil," *Procedia Engineering*, vol. 143, pp. 363–370, 2016.

[2] E. M. B. De Guzman and M. C. Alfaro, "Laboratory-scale model studies on corduroy-reinforced road embankments on peat foundations using transparent soil," *Transportation Geotechnics*, vol. 16, pp. 1–10, 2018.

[3] W. Zhang, H. Zhong, Y. Xiang, D. Wu, Z. Zeng, and Y. Zhang, "Visualization and digitization of model tunnel deformation via transparent soil testing technique," *Underground Space*, 2020.

[4] Y. Xiang, H. Liu, W. Zhang, J. Chu, D. Zhou, and Y. Xiao, "Application of transparent soil model test and DEM simulation in study of tunnel failure mechanism," *Tunnelling And Underground Space Technology*, vol. 74, pp. 178–184, 2018.

[5] F. M. Ezzein and R. J. Bathurst, "A new approach to evaluate soil-geosynthetic interaction using a novel pullout test apparatus and transparent granular soil," *Geotextiles and Geomembranes*, vol. 42, no. 3, pp. 246–255, 2014.

[6] M. G. Iskander, J. Liu, and S. Sadek, "Transparent amorphous silica to model clay," *Journal of Geotechnical and Geoenvironmental Engineering*, vol. 128, no. 3, pp. 262–273, 2002.

[7] J. Liu, M. G. Iskander, and S. Sadek, "Consolidation and permeability of transparent amorphous silica," *Geotechnical Testing Journal*, vol. 26, no. 4, pp. 11056–11401, 2003.

[8] B. Yuan, M. Sun, L. Xiong, Q. Luo, S. P. Pradhan, and H. Li, "Investigation of 3D deformation of transparent soil around a laterally loaded pile based on a hydraulic gradient model test," *Journal of Building Engineering*, vol. 28, p. 101024, 2020.

[9] M. G. Iskander, S. Sadek, and J. Liu, "Optical measurement of deformation using transparent silica gel to model sand," *International Journal of Physical Modelling in Geotechnics*, vol. 2, no. 4, pp. 13–26, 2002.

[10] I. L. Guzman, M. Iskander, and S. Bless, "Observations of projectile penetration into a transparent soil," *Mechanics Research Communications*, vol. 70, pp. 4–11, 2015.

[11] S. Sadek, M. G. Iskander, and J. Liu, "Accuracy of digital image correlation for measuring deformations in transparent media," *Journal of Computing in Civil Engineering*, vol. 17, no. 2, pp. 88–96, 2003.

[12] M. Iskander, S. Sadek, and J. Liu, "Soil structure interaction in transparent synthetic soils using digital image correlation," *proc*, vol. 03-2360, pp. 1–23, 2003.

[13] S. Kashuk, S. R. Mercurio, and M. Iskander, "Visualization of dyed NAPL concentration in transparent porous media using color space components," *Journal of Contaminant Hydrology*, vol. 162-163, pp. 1–16, 2014.

[14] G. Q. Kong, L. D. Zhou, and Z. T. Wang, "Shear modulus and damping ratios of transparent soil manufactured by fused quartz," *Materials Letters*, vol. 182, pp. 257–259, 2016.

[15] G. Xu, *Research on the mechanism and evolution law of rock deformation and cracking around deep tunnels*, China Univ. Min. Tech, 2011.

[16] M. Ahmed and M. Iskander, "Evaluation of tunnel face stability by transparent soil models," *Tunnelling & Underground Space Technology Incorporating Trenchless Technology Research*, vol. 27, no. 1, pp. 101–110, 2012.

[17] L. Wei, Q. Xu, S. Wang, C. Wang, and J. Chen, "Development of transparent cemented soil for geotechnical laboratory modelling," *Engineering Geology*, vol. 262, p. 105354, 2019.

[18] J. Zhang, *Study on the development of transparent similar materials for rock mass and its experimental applications*, J. China University Min. Techn, 2014.

[19] W. Ye, *Experiment study of internal 3d crack propagation in brittle and transparent rock-like material*, Chongqing University, 2016.

[20] J. Fu, W. Zhu, and X. Luo, "Study on failure process of fractured rock by using a new material containing three-dimensional internal fracture surfaces," *Zhongnan Daxue Xuebao (Ziran Kexue Ban)/Journal of Central South University (Science and Technology)*, vol. 45, no. 9, pp. 3257–3263, 2014.

[21] L. I. Yuanhai, Z. Lin, and X. Qin, *Study of development of transparent rock mass for physical similarity experiment and its mechanical properties*, Journal of China University of Mining & Technology, 2015.

[22] Y. Q. Hu, Y. S. Zhao, and D. Yang, "Simulation theory and method of 3D solid-liquid coupling," Journal of Liaoning Technical University, 2007.

[23] J. Sun and J. Liu, "Visualization of tunnelling-induced ground movement in transparent sand," *Tunnelling and Underground Space Technology*, vol. 40, pp. 236–240, 2014.